Experimental Mechanics
https://doi.org/10.1007/s11340-018-0433-0

Analysis of the Influence of the Thickness and the Hole Radius on the Calibration Coefficients in the Hole-Drilling Method for the Determination of Non-uniform Residual Stresses

J.M. Alegre[1] · A. Díaz[1] · I.I. Cuesta[1] · J.M. Manso[2]

Received: 15 May 2018 / Accepted: 16 September 2018

Abstract
The Hole-Drilling method is a semi-destructive technique useful for obtaining residual stress distributions by drilling and measuring relieved strains. The standard for this method, i.e., ASTM E837 – 13a, is based on the Integral Method and facilitates obtaining the coefficient matrices required to solve the inverse problem and to calculate the residual stress at depths of up to 1.00 mm. A possible deviation from the coefficients given by this standard is searched when the piece has a small thickness or the hole diameter is not 2.00 mm. FEM simulations are performed with the aim of analysing these effects and proposing new matrices, expressions and correlations for conditions outside the usual thickness and diameter limits. A parametric sweep over a wide range of thicknesses and hole diameters has been implemented in ANSYS to establish a consistent and automated numerical procedure for widening the applicability of the Hole-Drilling method.

Keywords Hole-drilling · Residual stress · Finite element method · Strain gauges

Introduction

Residual stresses are present in many industrial components due to fabrication processes. For example, welding induces thermal expansion near the heat-affected zone and thereby introduces residual stress, which can promote unexpected failure [1, 2]; machining or cold-forming can also generate residual stresses [3] that affect fatigue life [4]. However, sometimes, a compressive residual stress distribution is introduced with the objective of improving the fatigue life [5–7]. Therefore, knowing the actual stress state of a piece is fundamental to evaluating its integrity during its service life. Measurement techniques can be classified into destructive and non-destructive methods [8]. Although the Hole-Drilling method removes material from the target piece, the hole is usually so small in comparison with the piece's dimensions that the component's integrity is almost unaffected; such measurements may be regarded as an intermediate situation between destructive and non-destructive, i.e., semi-destructive [8].

The Hole-Drilling method comprises three stages: drilling operation, registration of relieved strains and stress calculation. The relieved strains might be measured using optical methods, such as Digital Image Correlation or interferometry [9]. However, those methods have not been standardised in the Hole-Drilling framework; instead, strain gauge rosettes are considered in ASTM E837 – 13a [10]. Here, rosettes comprising three strain gauges are analysed, but it should be noted that other common configurations include a four-gauge rosette (for plasticity correction [11–13]) and a special-purpose six-gauge rosette (for measurements requiring high sensitivity [14]). Rosettes of types A and B are shown in Fig. 1. Both have two strain gauges forming a 90° angle, but while rosette A has the third gauge on the prolongation of their bisector, i.e., in the opposite quadrant, in rosette B, this third gauge forms a 45° angle with the other two, i.e., it is in the same quadrant.

The rosette dimensions are standardised, giving three independent parameters: the rosette diameter *D*, the gauge length *GL* and the gauge width *GW*. The gauge width of a type-B rosette must be less than the *GW* of a type-A rosette because three strain gauges are placed in the same quadrant. In addition, radii comprising the rosette are

✉ A. Díaz
adportugal@ubu.es

[1] Structural Integrity Group, Escuela Politécnica Superior, Universidad de Burgos, Av Cantabria s/n, 09006 Burgos, Spain

[2] SUCONS Research Group, Escuela Politécnica Superior, Universidad de Burgos, C/Villadiego s/n, 09001 Burgos, Spain

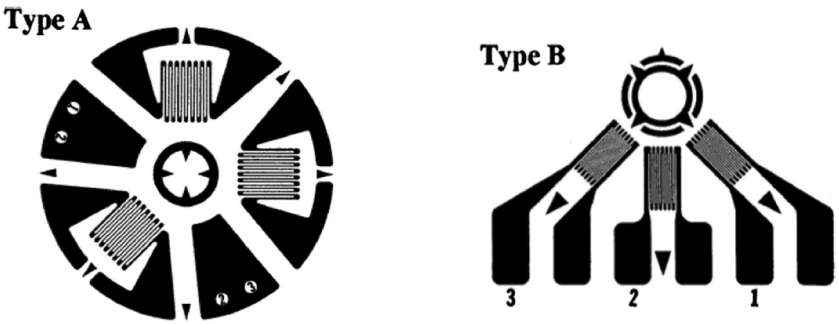

Fig. 1 Types of 3-strain-gauge rosettes [10]

usually defined, especially for node placement in Finite Element simulations:

$$R_1 = \frac{1}{2}(D - GL) \tag{1}$$

$$R_2 = \frac{1}{2}(D + GL) \tag{2}$$

All the geometric parameters are graphically defined in Fig. 4. This paper focuses on the last stage of the Hole-Drilling procedure, i.e., the numerical relationship between the relieved strains and the actual residual stress distribution. There are several calculation algorithms whose objective is to relate the relieved strains and the residual stress [15]. ASTM E837 – 13a standardises the integral approach and establishes a procedure for obtaining the non-uniform residual stresses in the first millimetre of depth. Following the standard, a minimum thickness is required for a workpiece to be considered "thick" [10] and for the non-uniform stress calibration coefficients to be valid.

The Integral Method is a mathematical approach based on the superposition principle [16]; this algorithm is reviewed in "Results and Discussion" section. The main objective of this study is to discuss the procedure found in ASTM E837 – 13a and to widen its range of applicability. Matrices of calibration coefficients are re-evaluated to consider the influences of the thickness and the hole diameter. All calculations are made using Finite Element simulations, and an automated procedure for parametric evaluation is established.

Integral Method

The relieved strain registered at drilling depth h depends on the stress at depth $\sigma(z)$ and can be found by integrating over every depth increment dz [17]:

$$\varepsilon(h) = \frac{1+\nu}{E}\int_0^h G(z,h)\sigma(z)dz \tag{3}$$

where $G(z, h)$ are so-called kernel functions, which quantify the sensitivity of the measured strain to the stress at depth z; the deeper the stress applied is, the lower its influence on the relieved strains measured at the surface. Equation (3) constitutes an inverse problem; therefore, obtaining the stress distribution is not straightforward. The Integral Method is based on transforming the continuous problem into a set of discrete equations. Assuming a three-strain-gauge rosette, the following three combinations of strains are usually defined [10]:

$$p = \frac{\varepsilon_3 + \varepsilon_1}{2} \qquad q = \frac{\varepsilon_3 - \varepsilon_1}{2} \qquad t = \frac{\varepsilon_3 + \varepsilon_1 - 2\varepsilon_2}{2} \tag{4}$$

Because the registered strain evolves, these combinations are actually functions of depth or vectors whose components correspond to each step during material removal. The corresponding stress combinations are:

$$P = \frac{\sigma_3 + \sigma_1}{2} \qquad Q = \frac{\sigma_3 - \sigma_1}{2} \qquad T = \tau_{13} \tag{5}$$

An integral equation similar to (3) that includes the kernel functions $A(z, h)$ and $B(z, h)$ is defined for each stress-strain pair:

$$p(h) = \frac{1+\nu}{E}\int_0^h A(z,h)P(z)dz \tag{6}$$

$$q(h) = \frac{1}{E}\int_0^h B(z,h)Q(z)dz \tag{7}$$

$$t(h) = \frac{1}{E}\int_0^h B(z,h)T(z)dz \tag{8}$$

To handle this set of inverse problems, the equations are transformed into a discrete matrix system in which p_i, q_i and t_i are the strain combinations obtained experimentally for each depth increment i [10]:

$$p_i = \frac{1+\nu}{E}\sum_{j=1}^{j=i} \overline{a}_{ij}P_j \tag{9}$$

$$q_i = \frac{1}{E}\sum_{j=1}^{j=i} \overline{b}_{ij} Q_j \tag{10}$$

$$t_i = \frac{1}{E}\sum_{j=1}^{j=i} \overline{b}_{ij} T_j \tag{11}$$

By solving these three matrix systems, the unknown vectors P_j, Q_j and T_j are found; finally, using the equations in (5), the stress distribution can be obtained for each depth j in the coordinate system defined by the gauges. The non-dimensional coefficients $\overline{a}_{ij}$ and $\overline{b}_{ij}$ represent the strain relaxation after removal step i due to unit stress at depth j. They are related to the kernel functions through the following expressions:

$$\overline{a}_{ij} = \int_{z_{j-1}}^{z_j} A(z, h_i)dz \tag{12}$$

$$\overline{b}_{ij} = \int_{z_{j-1}}^{z_j} B(z, h_i)dz \tag{13}$$

In the present study, the strain relaxation matrices are examined using FEM simulations. However, sometimes, the cumulative strain relaxation coefficients are found instead. In the equi-biaxial situation (i.e.,p_i, P_j) the difference in physical meaning between $\overline{a}_{ij}$ and $\overline{A}_{ij}$ is shown in Fig. 2. The cumulative strain relaxation coefficients are defined by [18]:

$$\overline{A}_{ij} = \int_{0}^{z_j} A(z, h_i)dz \tag{14}$$

$$\overline{B}_{ij} = \int_{0}^{z_j} B(z, h_i)dz \tag{15}$$

Range of Applicability of ASTM E837 – 13a

Non-uniform stresses can only be calculated for "thick" pieces according to the ASTM standard. The recommended workpiece thickness, hole diameter and depth step size are shown in Table 1. These values correspond to the most commonly used rosettes, types A and B, with a diameter of 5.13 mm:

Table 1 Recommendations for workpiece thickness, hole diameter and depth step size in ASTM E837-13a [10]

Max. thickness for a "thin workpiece"	Uniform stress		
	Min. D_0	Max. D_0	Step size
1.03	1.52	2.54	0.10
Min. thickness for a "thick workpiece"	Non-uniform stress		
	Min. D_0	Max. D_0	Step size
5.13	1.88	2.12	0.05

To sum up, when applying the standard the following aspects must be considered:

- Residual stresses can only be calculated in a 1 mm layer.
- Non-uniform stresses can only be calculated for pieces that are more than 5.13 mm thick.
- Plasticity effects are not included because this standard is based on the superposition principle.

In addition, the $\overline{a}_{ij}$ and $\overline{b}_{ij}$ matrices are tabulated only for $D_0 =$ 2 mm, and a correction factor is introduced for other hole diameters. Here, possible deviations from this correction are evaluated. A discussion of the limitations associated with plasticity is beyond the scope of the present paper; information regarding plastic correction can be found in other studies [12, 20].

Finite Element Procedure and Validation

The Finite Element Method has already been used by many authors for determining $\overline{a}_{ij}$ and $\overline{b}_{ij}$, the coefficients of the calibration matrices [15, 21–25]. The well-known finite elements code ANSYS is used, and a three-dimensional model is created. As a consequence of the symmetry conditions, only a quarter of the model is necessary. An example of the mesh developed is shown in Fig. 3. An element size of 0.05 mm is used in the inner surface of the simulated drilled hole where the loads are applied. Distributed stresses have been applied in

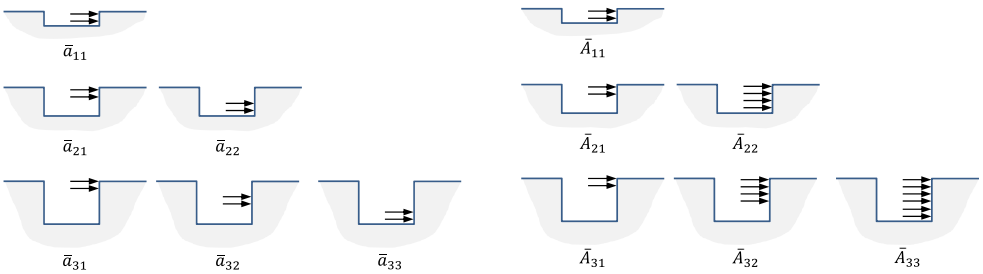

Fig. 2 Physical meaning of the strain relaxation and cumulative strain relaxation coefficients (adapted from [19])

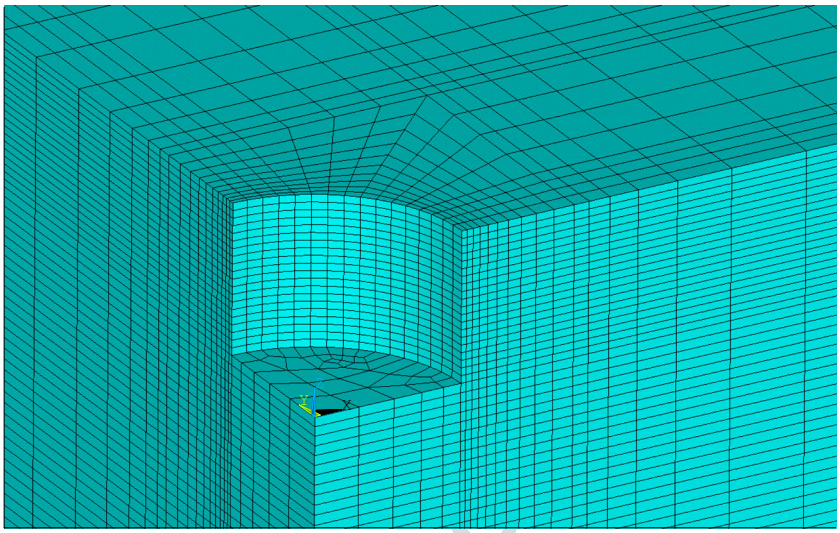

Fig. 3 Simulated drilled hole: Finite Element geometry and mesh

0.05-mm increments, following [15]; finer mesh was investigated but results were practically unaffected so the element size of 0.05 mm is considered for all simulations. A minimum of 16 elements in the hoop direction is used to model a quarter of the workpiece. The element type selected is SOLID185, which is commonly used for three-dimensional modelling of solid structures. This element type features plasticity, stress stiffening, large deflection, and large strain capabilities. Although in this study, only a linear elastic analysis is required, the model can be used to consider non-linear effects.

The main fixed dimensions used for the workpiece simulation are initial diameter of the gauge circle $D = 5.13\ mm$, gauge length $GL = 1.59\ mm$, and external dimension of the workpiece $D_{\max} = 12\ mm$. The thickness of the workpiece and the diameter of the drilled hole are modified for each simulation with the objective of performing a parametric study. The dimensions are illustrated in Fig. 4.

The strain measured by the strain gauges is obtained from the radial displacement of the initial and final points of the middle axis of the strain gauge, according to $[u_x(R_2) - u_x(R_1)]/GL$. It must be noted that this measured deformation constitutes a simplification because the gauge width effect is neglected. Additionally, only stresses on the x-y plane have been considered; stresses at the hole's bottom face have been neglected, though they can appear due to material removal.

However, the validation presented above demonstrates that the approximation is good enough for calculating the strain based on the strain gauge measurement.

An initial validation analysis is performed. For this purpose, the coefficients obtained for the isotropic stresses $\overline{a}_{ij}$ and for the shear stresses $\overline{b}_{ij}$ are compared with those provided in ASTM E837 – 13a. The obtained Hole-Drilling calibration coefficients in the matrix, $\overline{a}_{ij}$ and $\overline{b}_{ij}$, are presented in Figs. 5 and 6, respectively, together with the calibration coefficients collected in ASTM E837 – 13a that correspond to a type-B rosette. That type of rosette is chosen for validation because its gauge width is smaller than that of a type-A rosette; therefore, behaviour that is more similar to the present FE simulations is expected. Very good agreement between the coefficients is observed. The results corresponding to intermediate hole depths (h = 0.20 mm, 0.25 mm, etc.) are omitted for clarity.

Results and Discussion

With the aim of assessing the effects of the thickness and the hole radius, a parametric study was conducted. Considering the values

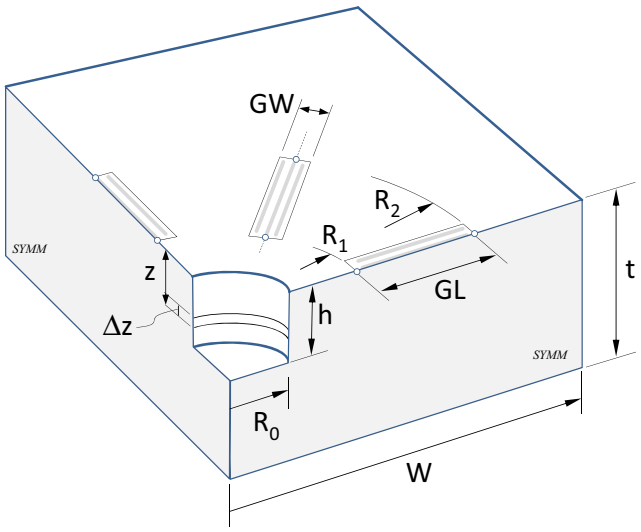

Fig. 4 Main dimensions of the simulated geometry (not to scale)

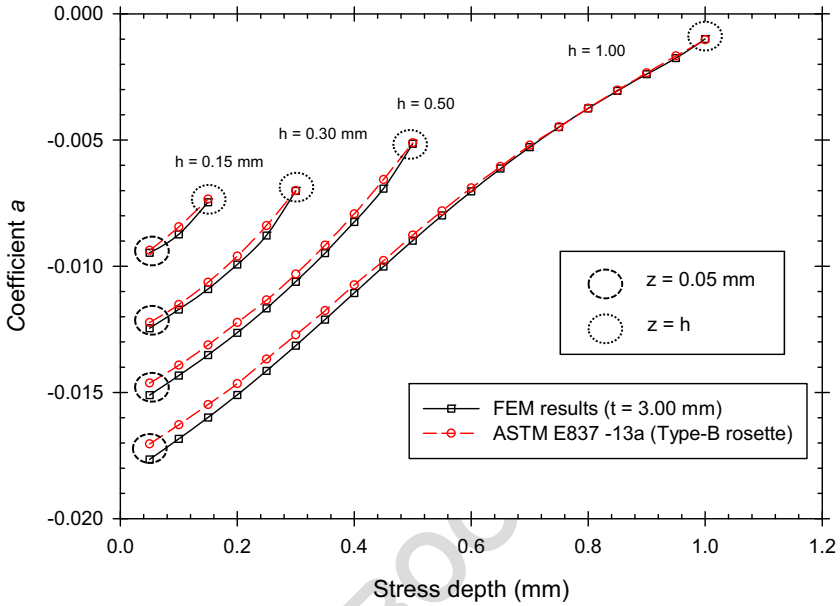

Fig. 5 Comparison between matrix $\overline{a}_{ij}$ for a type-B rosette (from Table 6(a) in ASTM E837 – 13a) and the FE simulation with R_0 = 1.00 mm and thickness = 3.00 mm

shown in Table 2, a parametric sweep over every possible combination was performed, giving a total of 40 simulations.

The results corresponding to a 1.00 mm hole radius and a 3.00 mm thickness have already been shown for validation purposes. In the following sections, even though 40 complete matrices were obtained, only the most substantial results are presented. Selected complete matrices for small thicknesses are given in Appendix 1, as the objective of this paper is to extend the applicability of ASTM E837-13a using the matrix Integral Method.

Effect of the Thickness

For a fixed hole radius of 1.00 mm, as in ASTM E837-13a, the effect of the thickness on the calibration coefficients was evaluated. The graph for all the simulated thicknesses shown in Fig. 7 is for the row corresponding to a hole depth of 1.00 mm, i.e., the last row of the $\overline{a}_{ij}$ matrix, which demonstrates that the trend is asymptotic. This result explains why the standard establishes a minimum workpiece thickness, which is equal to a rosette diameter of 5.13 mm,

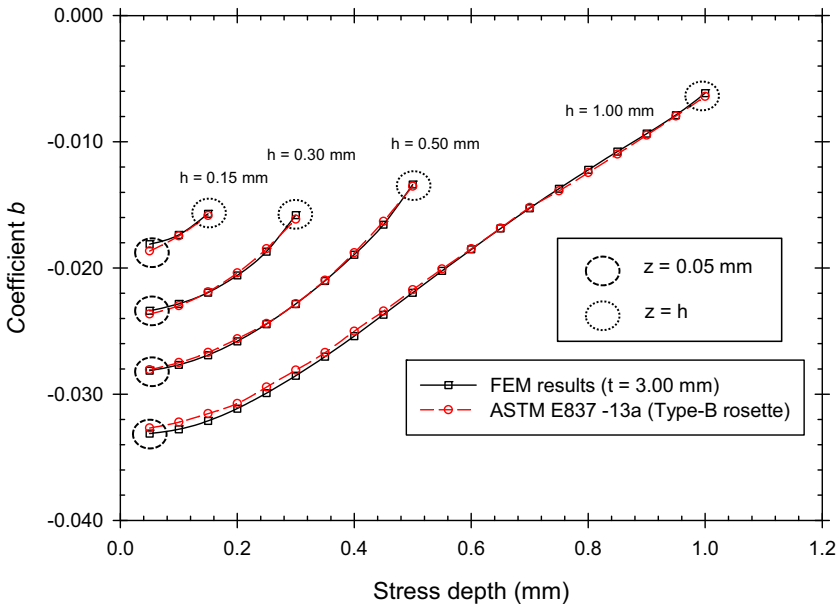

Fig. 6 Comparison between matrix $\overline{b}_{ij}$ for a type-B rosette (from Table 6(a) in ASTM E837 – 13a) and the FE simulation with R_0 = 1.00 mm and thickness = 3.00 mm

Table 2 Simulated values of the hole radius and the workpiece thickness

Parameter	Range evaluated
Hole radius: R_0 [mm]	0.25, 0.50, 0.75, 1.00, 1.25
Thickness: t [mm]	1.05, 1.10, 1.25, 1.50, 2.00, 3.00, 5.00, 10.00

as shown in Fig. 7. It is worth noting that for small thicknesses, two different curvatures are obtained in the evolution of the effect of the thickness; they depend on whether the coefficient corresponds to a stress applied near the bottom of the hole (top lines, near $z = 1.00$ mm) or next to the workpiece's surface (bottom lines, near $z = 0.05$ mm). This shape of $\overline{a}_{ij}$ Fig. 7 is caused by the localised bending [26] and the change in behaviour is delimited by the coefficient corresponding to $z = 0.60$ mm, approximately. This change is attributed to the influence of the free surface at the bottom: for a very low thickness, the constriction associated rwith the bottom is very weak and the deformation increases to a negative value when stress is applied near $z = 0.05$ mm (more compression in the strain gauge surface) and even to a positive value when stress is applied near $z = 1.00$ mm (traction at the the surface to which the straing gauge is applied).

For the coefficient line corresponding to $z = 0.05$ mm, a similar tendency is observed for the values of the $\overline{b}_{ij}$ matrix: compressive deformation increases for low thicknesses because the hole is less constrained. However, due to the association of the $\overline{b}_{ij}$ matrix with a shear stress state, positive coefficients are not found for $z = 1.00$ mm and the neighbouring lines. The same curvature is thus found for every coefficient in Fig. 8.

For both calibration coefficient matrices, it can be concluded that the thickness limitation of 5.13 mm proposed by the standard is too restrictive. A very smooth coefficient change is found and the values in the standard are only completely invalid for thicknesses less than 3.00 mm. Complete matrices for thicknesses 1.05, 1.50 and 2.00 mm are included in Appendix 1.

Effect of the Hole Diameter

The hole diameter is determined by the end mill dimension. Although commercial Hole-Drilling devices feature a wide range of cutter diameters, ASTM E837 – 13a focuses on a general-purpose 1.00 mm radius for the drill, so the applicability of the calibration coefficients lies in a range of ±0.06 mm: R_0 between 0.94 and 1.06 mm. Figure 9 represents the change in the $\overline{a}_{ij}$ matrix, with the coefficient corresponding to $R_0 = 1.00$ mm on the x-axis, and the new coefficient for a different radius on the y-axis. Hence, for $R_0 > 1.00$ mm, the points lie below a line with slope one, whereas for $R_0 < 1.00$ mm, the coefficients lie above this line. This result demonstrates how calibration coefficients (or their absolute values) decrease with smaller holes and increase with larger ones. This behaviour may be attributed to the fact that if the ratio D_0/D is very large, the strain is measured close to the edge of the hole, and hence, the

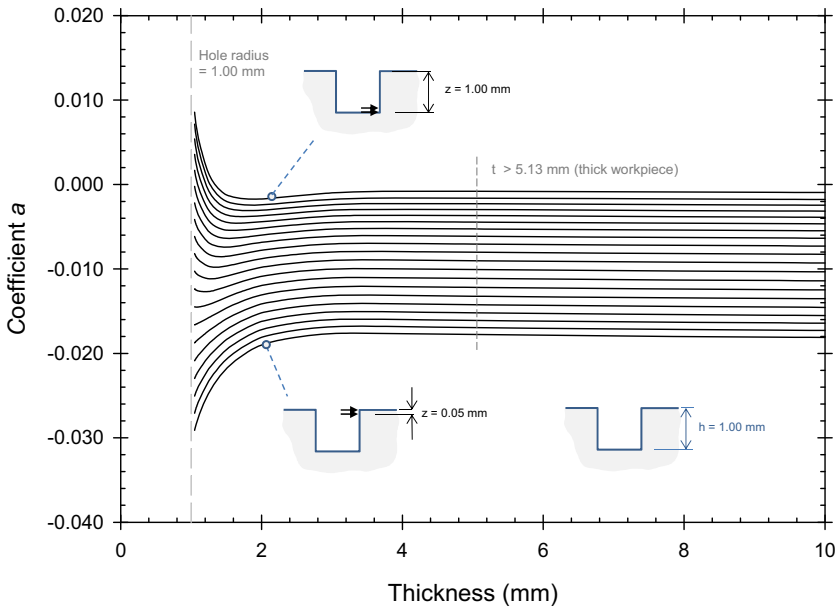

Fig. 7 Effect of the thickness on the coefficients $\overline{a}(z,h)$ for hole depth $h = 1.00$ mm and hole radius $R_0 = 1.00$ mm. Coefficients correspond to the tenth row of the $\overline{a}(z,h)$ matrix, with increasing stress depth from bottom ($z = 0.05$ mm) to top ($z = 1.00$ mm)

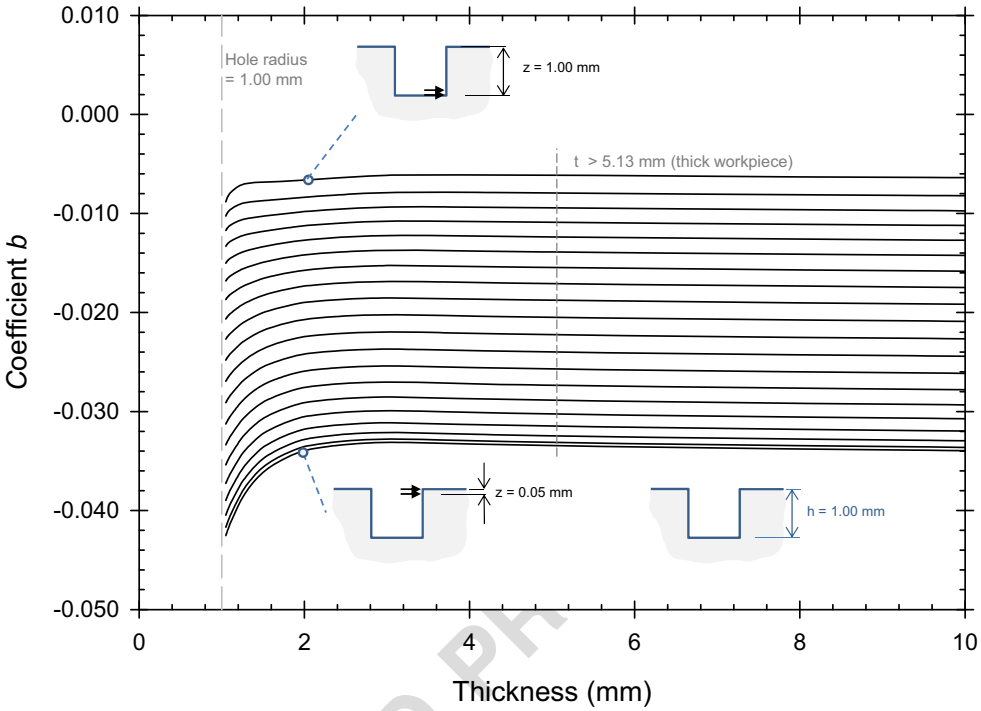

Fig. 8 Effect of the thickness on the coefficients $\overline{b}(z,h)$ for hole depth h = 1.00 mm and hole radius R_0 = 1.00 mm. Coefficients correspond to the tenth row of the $\overline{a}(z,h)$ matrix, with increasing stress depth from bottom (z = 0.05 mm) to top (z = 1.00 mm)

deformation must be higher. In a similar way, for R_0 < 1.00 mm, the results show that the calibration coefficients are less sensitive to the hole size. Again, a bulk constraint may also have a role. It must be recalled that every simulation presented in Figs. 9, 10, 11, and 12 is based on a very thick workpiece (t = 10.00 mm).

A similar effect is found for the $\overline{b}_{ij}$ matrix, but an even higher increase in the negative deformation is observed for large values of R_0. The curves in Figs. 9 and 10 are not easy to fit using a linear regression, even though the proposed correction in ASTM E837 – 13a is as follows [10]:

$$\overline{a}_{ij,R_0} = \left(\frac{R_0}{1.00\ \text{mm}}\right)^2 \overline{a}_{ij,1.00\ \text{mm}} \tag{16}$$

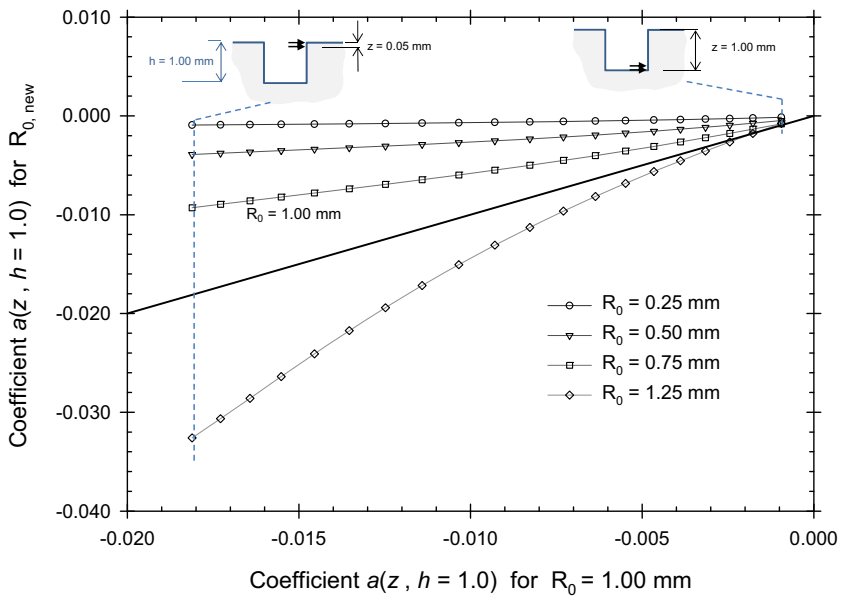

Fig. 9 Effect of the hole radius on the coefficients $\overline{a}(z,h)$ for hole depth h = 1.00 mm and thickness t = 10.00 mm

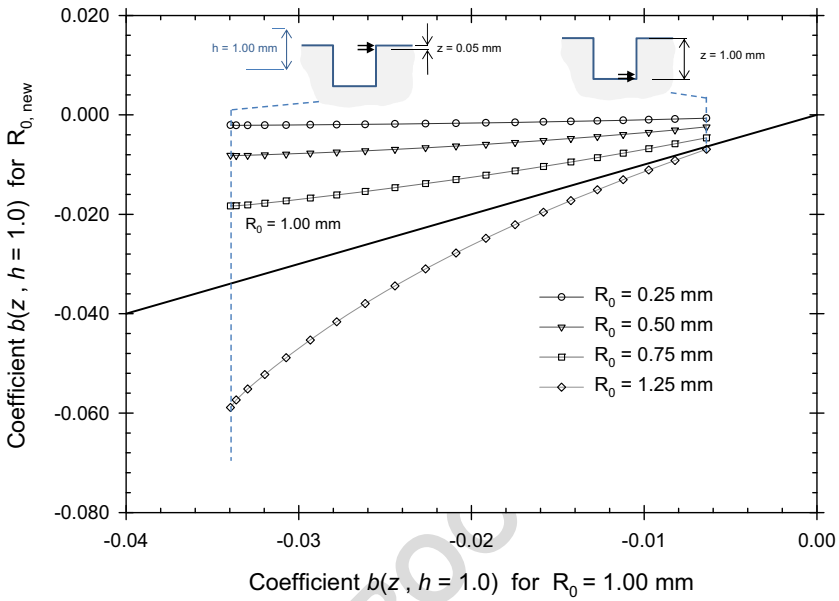

Fig. 10 The effect of the hole radius on the coefficients $\overline{b}(z,h)$ for hole depth h = 1.00 mm and thickness t = 10.00 mm

With the aim of evaluating the apparent deviation of the simulated coefficients from the correction proposed in equation (16), the ratio $\overline{a}_{R_0}/\overline{a}_{1.00\ \mathrm{mm}}$ is graphed against the hole radius in Fig. 11. The coefficients obtained through FE simulations with different hole sizes are also compared with the correction proposed by the standard, i.e., equation (16). The latter, which is a parabola, is a reasonably good prediction for hole radii near 1.00 mm or for coefficients corresponding to a stress applied near the free surface, i.e., close to z = 0.05 mm. In contrast, coefficients corresponding to a stress applied near the bottom of the hole, i.e., close to z = 1.00 mm, are found to deviate significantly from the correction given in ASTM E837 – 13a. Despite this, the measurements taken during drilling at sub-surface depths are highly susceptible to measurement errors, so that deviations in numeri-

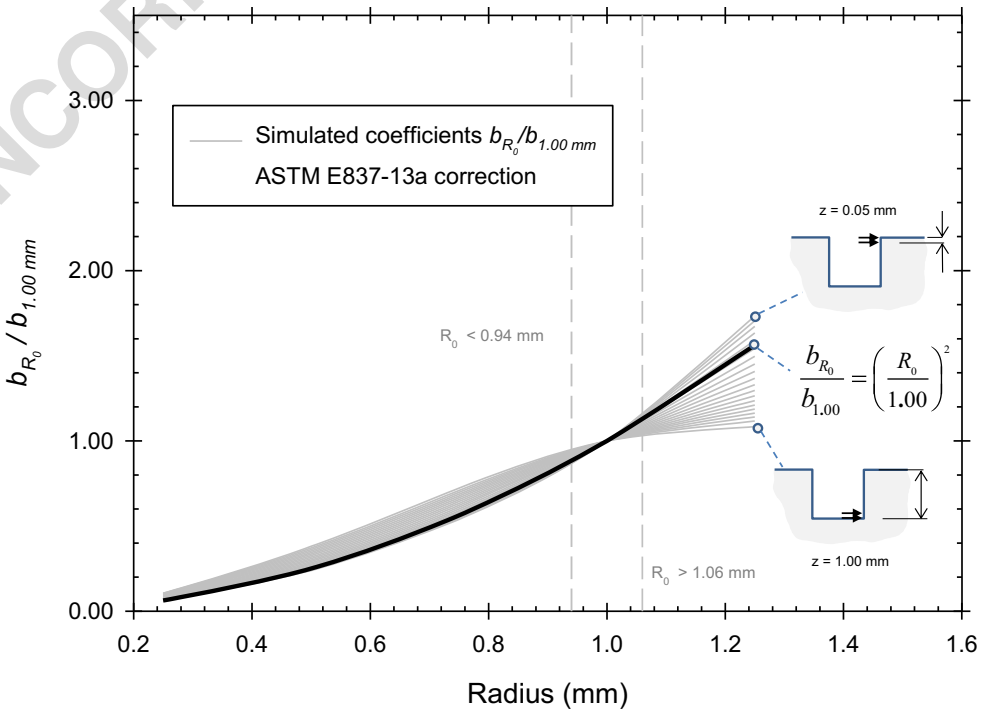

Fig. 11 Deviation from the hole diameter correction proposed by ASTM E837 – 13a for hole depth h = 1.00 mm and thickness t = 10.00 mm

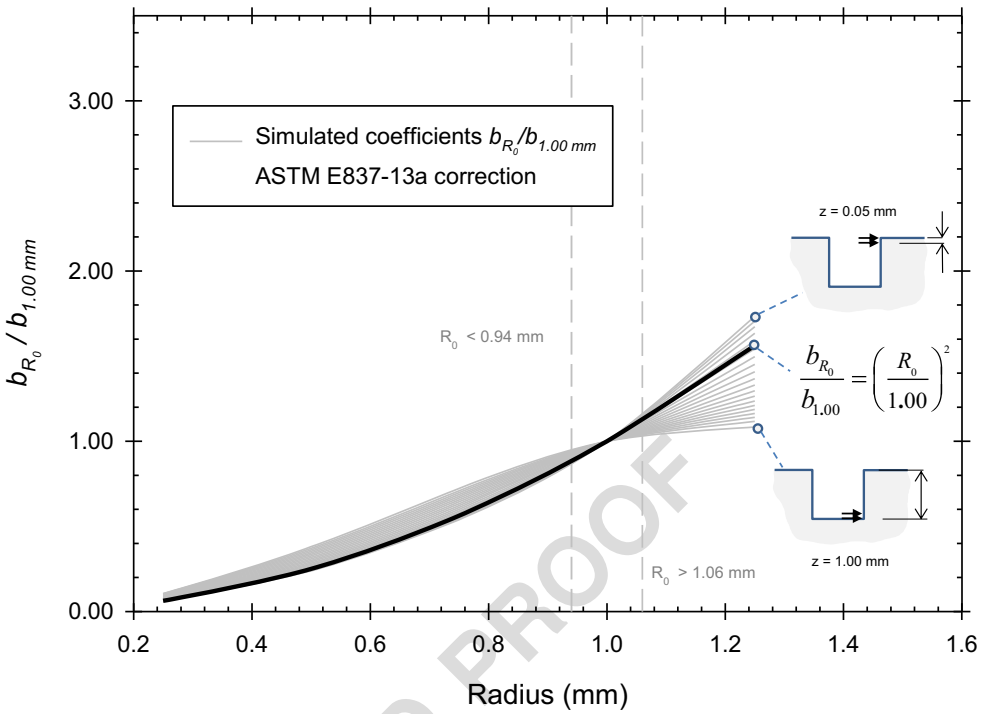

Fig. 12 Deviation from the hole diameter correction proposed by ASTM E837 – 13a for hole depth h = 1.00 mm and thickness t = 10.00 mm

cal values may be acceptable to a certain degree since their contribution to the overall experimental error is less than from the measurement errors. The correction by diameter considered by the standard, although imprecise, can be valid taking into account that regularization tends to reduce these effects.

Following the same procedure, Fig. 12 shows a comparison between the simulated values of $\overline{b}_{R_0}/\overline{b}_{1.00\ mm}$ and the correction recommended by the standard. Behaviour similar to that found in Fig. 11 is obtained. However, note how coefficients corresponding to different stress locations are concentrated in a narrower spectrum, especially for coefficients close to z = 1.00 mm. Consequently, it can be assumed here that the prediction given by ASTM E837 – 13a is better for the "b" matrix than for the "a" matrix.

Conclusions

A Finite Element procedure was validated as a powerful tool for finding coefficient matrices in the Integral Method framework as a first step in measuring residual stresses using the Hole-Drilling method. Using ANSYS, the results were compared with the coefficients given by ASTM E837 – 13a; they were in very good agreement for type-B rosettes. It can be deduced from this correspondence that the present simulations are valid for thin strain gauges. In future extensions, the gauge width will be included as an influential parameter.

In addition, the limits on the thickness and hole radius were studied and discussed. The definition of a "thick" workpiece in ASTM E837 – 13a was attributed to the critical change in the calibration coefficients for small thicknesses, which is physically related to the constraints. The presented results and the matrices given in Appendix 1 are expected to overcome this limitation to experimentally determine the non-uniform residual stress distribution in a thin workpiece. The influence of the hole diameter was also analysed with a focus on a critical revision of the correction proposed in ASTM E837 – 13a. It was concluded that the adjustment for a hole diameter different than 2.00 mm used by the standard might be improved because the coefficients found in the FE simulations deviated significantly from this correction. The observed deviation is especially important for large hole diameters. As a general conclusion, a particular matrix must be obtained through the exposed automated numerical procedure when the analysed workpiece is too thin (t < 3.00 mm) or when the hole diameter is relatively large (D_0 > 1.1 mm).

Acknowledgments The authors gratefully acknowledge financial support from the Junta of Castile and Leon through grant no. BU053U16.

Appendix 1: Matrices for Small Thickness

All calibration matrices correspond to a strain rosette diameter $D = 5.13$ mm and a hole diameter $D_0 = 2.00$ mm.

Table 3 Calibration matrix $\overline{a}_{ij}$ for thickness $t = 1.05$ mm

Stress depth / Hole depth mm	0.05	0.1	0.15	0.2	0.25	0.3	0.35	0.4	0.45	0.5
0.05	−0.01286									
0.10	−0.01558	−0.01352								
0.15	−0.01789	−0.01614	−0.01379							
0.20	−0.01998	−0.01819	−0.01628	−0.01373						
0.25	−0.02181	−0.02001	−0.01810	−0.01605	−0.01338					
0.30	−0.02339	−0.02156	−0.01967	−0.01765	−0.01550	−0.01277				
0.35	−0.02472	−0.02286	−0.02095	−0.01898	−0.01689	−0.01468	−0.01196			
0.40	−0.02580	−0.02392	−0.02200	−0.02003	−0.01800	−0.01586	−0.01364	−0.01097		
0.45	−0.02665	−0.02475	−0.02283	−0.02087	−0.01885	−0.01678	−0.01463	−0.01242	−0.00984	
0.50	−0.02729	−0.02539	−0.02346	−0.02150	−0.01949	−0.01745	−0.01537	−0.01324	−0.01107	−0.00862
0.55	−0.02774	−0.02584	−0.02392	−0.02196	−0.01997	−0.01794	−0.01589	−0.01383	−0.01174	−0.00964
0.60	−0.02804	−0.02615	−0.02423	−0.02228	−0.02029	−0.01828	−0.01626	−0.01422	−0.01219	−0.01016
0.65	−0.02822	−0.02633	−0.02442	−0.02248	−0.02051	−0.01851	−0.01649	−0.01448	−0.01248	−0.01050
0.70	−0.02832	−0.02643	−0.02453	−0.02259	−0.02063	−0.01864	−0.01664	−0.01464	−0.01265	−0.01069
0.75	−0.02835	−0.02647	−0.02457	−0.02264	−0.02068	−0.01870	−0.01670	−0.01471	−0.01274	−0.01079
0.80	−0.02836	−0.02649	−0.02459	−0.02265	−0.02069	−0.01871	−0.01672	−0.01473	−0.01275	−0.01081
0.85	−0.02839	−0.02650	−0.02459	−0.02266	−0.02069	−0.01870	−0.01670	−0.01470	−0.01272	−0.01076
0.90	−0.02847	−0.02656	−0.02464	−0.02268	−0.02069	−0.01868	−0.01666	−0.01464	−0.01263	−0.01066
0.95	−0.02867	−0.02673	−0.02476	−0.02276	−0.02073	−0.01868	−0.01662	−0.01456	−0.01252	−0.01050
1.00	−0.02911	−0.02709	−0.02505	−0.02298	−0.02088	−0.01875	−0.01662	−0.01449	−0.01237	−0.01027

Stress depth / Hole depth mm	0.55	0.60	0.65	0.70	0.75	0.80	0.85	0.90	0.95	1.00
0.55	−0.00732									
0.60	−0.00814	−0.00597								
0.65	−0.00853	−0.00660	−0.00457							
0.70	−0.00877	−0.00687	−0.00502	−0.00314						
0.75	−0.00888	−0.00700	−0.00518	−0.00340	−0.00166					
0.80	−0.00890	−0.00703	−0.00521	−0.00344	−0.00173	−0.00010				
0.85	−0.00884	−0.00696	−0.00513	−0.00334	−0.00162	0.00004	0.00156			
0.90	−0.00871	−0.00681	−0.00494	−0.00313	−0.00136	0.00035	0.00198	0.00342		
0.95	−0.00851	−0.00655	−0.00464	−0.00276	−0.00093	0.00086	0.00259	0.00423	0.00562	
1.00	−0.00820	−0.00616	−0.00415	−0.00217	−0.00022	0.00169	0.00357	0.00540	0.00714	0.00856

Table 4 Calibration matrix $\overline{b}_{ij}$ for thickness $t = 1.05$ mm

Stress depth / Hole depth mm	0.05	0.1	0.15	0.2	0.25	0.3	0.35	0.4	0.45	0.5
0.05	−0.01743									
0.10	−0.02040	−0.01865								
0.15	−0.02304	−0.02174	−0.01932							
0.20	−0.02531	−0.02414	−0.02246	−0.01958						
0.25	−0.02748	−0.02636	−0.02484	−0.02276	−0.01947					
0.30	−0.02956	−0.02845	−0.02698	−0.02504	−0.02257	−0.01903				
0.35	−0.03133	−0.03025	−0.02882	−0.02700	−0.02478	−0.02211	−0.01843			
0.40	−0.03295	−0.03189	−0.03050	−0.02874	−0.02665	−0.02425	−0.02147	−0.01769		
0.45	−0.03435	−0.03332	−0.03196	−0.03026	−0.02824	−0.02599	−0.02347	−0.02059	−0.01681	
0.50	−0.03562	−0.03462	−0.03328	−0.03160	−0.02965	−0.02750	−0.02515	−0.02254	−0.01964	−0.01588
0.55	−0.03677	−0.03579	−0.03447	−0.03282	−0.03091	−0.02882	−0.02654	−0.02409	−0.02144	−0.01853
0.60	−0.03780	−0.03684	−0.03554	−0.03391	−0.03203	−0.02997	−0.02775	−0.02540	−0.02291	−0.02027
0.65	−0.03868	−0.03774	−0.03645	−0.03484	−0.03298	−0.03096	−0.02880	−0.02650	−0.02411	−0.02162
0.70	−0.03948	−0.03856	−0.03729	−0.03570	−0.03385	−0.03184	−0.02970	−0.02745	−0.02512	−0.02273
0.75	−0.04013	−0.03924	−0.03799	−0.03642	−0.03460	−0.03261	−0.03051	−0.02829	−0.02600	−0.02367
0.80	−0.04075	−0.03988	−0.03865	−0.03708	−0.03527	−0.03330	−0.03122	−0.02903	−0.02677	−0.02448
0.85	−0.04131	−0.04041	−0.03915	−0.03760	−0.03585	−0.03391	−0.03183	−0.02966	−0.02743	−0.02519
0.90	−0.04178	−0.04092	−0.03966	−0.03813	−0.03636	−0.03441	−0.03235	−0.03021	−0.02802	−0.02581
0.95	−0.04216	−0.04133	−0.04010	−0.03856	−0.03682	−0.03492	−0.03289	−0.03077	−0.02860	−0.02641
1.00	−0.04254	−0.04169	−0.04047	−0.03898	−0.03727	−0.03539	−0.03337	−0.03126	−0.02911	−0.02695
Stress depth / Hole depth mm	0.55	0.60	0.65	0.70	0.75	0.80	0.85	0.90	0.95	1.00
0.55	−0.01488									
0.60	−0.01743	−0.01390								
0.65	−0.01903	−0.01629	−0.01292							
0.70	−0.02029	−0.01780	−0.01517	−0.01201						
0.75	−0.02132	−0.01896	−0.01657	−0.01409	−0.01114					
0.80	−0.02219	−0.01991	−0.01764	−0.01539	−0.01309	−0.01039				
0.85	−0.02294	−0.02073	−0.01854	−0.01640	−0.01428	−0.01214	−0.00969			
0.90	−0.02361	−0.02144	−0.01932	−0.01725	−0.01524	−0.01328	−0.01134	−0.00921		
0.95	−0.02423	−0.02209	−0.02000	−0.01799	−0.01604	−0.01417	−0.01239	−0.01068	−0.00885	
1.00	−0.02480	−0.02270	−0.02066	−0.01870	−0.01681	−0.01502	−0.01331	−0.01172	−0.01026	−0.00882

Table 5 Calibration matrix $\bar{a}_{ij}$ for thickness $t = 1.50$ mm

Stress depth / Hole depth mm	0.05	0.1	0.15	0.2	0.25	0.3	0.35	0.4	0.45	0.5
0.05	−0.00913									
0.10	−0.01101	−0.00968								
0.15	−0.01258	−0.01154	−0.00995							
0.20	−0.01402	−0.01296	−0.01178	−0.01000						
0.25	−0.01530	−0.01425	−0.01310	−0.01178	−0.00986					
0.30	−0.01644	−0.01538	−0.01426	−0.01299	−0.01157	−0.00956				
0.35	−0.01744	−0.01637	−0.01525	−0.01404	−0.01268	−0.01118	−0.00915			
0.40	−0.01831	−0.01723	−0.01610	−0.01490	−0.01361	−0.01219	−0.01066	−0.00864		
0.45	−0.01905	−0.01796	−0.01683	−0.01564	−0.01437	−0.01302	−0.01157	−0.01004	−0.00806	
0.50	−0.01967	−0.01857	−0.01744	−0.01625	−0.01500	−0.01368	−0.01230	−0.01085	−0.00934	−0.00744
0.55	−0.02019	−0.01908	−0.01794	−0.01676	−0.01551	−0.01422	−0.01287	−0.01149	−0.01006	−0.00859
0.60	−0.02060	−0.01949	−0.01836	−0.01717	−0.01593	−0.01464	−0.01332	−0.01197	−0.01061	−0.00922
0.65	−0.02094	−0.01982	−0.01869	−0.01750	−0.01627	−0.01499	−0.01368	−0.01235	−0.01102	−0.00970
0.70	−0.02119	−0.02008	−0.01894	−0.01776	−0.01653	−0.01526	−0.01396	−0.01265	−0.01134	−0.01004
0.75	−0.02139	−0.02028	−0.01914	−0.01796	−0.01673	−0.01546	−0.01417	−0.01287	−0.01158	−0.01030
0.80	−0.02154	−0.02043	−0.01929	−0.01811	−0.01688	−0.01562	−0.01433	−0.01304	−0.01176	−0.01050
0.85	−0.02164	−0.02053	−0.01939	−0.01822	−0.01699	−0.01573	−0.01445	−0.01316	−0.01189	−0.01064
0.90	−0.02171	−0.02060	−0.01947	−0.01829	−0.01707	−0.01581	−0.01454	−0.01325	−0.01198	−0.01074
0.95	−0.02175	−0.02065	−0.01951	−0.01834	−0.01712	−0.01587	−0.01459	−0.01331	−0.01204	−0.01081
1.00	−0.02177	−0.02067	−0.01954	−0.01837	−0.01715	−0.01590	−0.01462	−0.01335	−0.01208	−0.01085

Stress depth / Hole depth mm	0.55	0.60	0.65	0.70	0.75	0.80	0.85	0.90	0.95	1.00
0.55	−0.00679									
0.60	−0.00781	−0.00613								
0.65	−0.00836	−0.00703	−0.00548							
0.70	−0.00877	−0.00750	−0.00626	−0.00483						
0.75	−0.00906	−0.00785	−0.00666	−0.00549	−0.00419					
0.80	−0.00927	−0.00808	−0.00694	−0.00583	−0.00475	−0.00357				
0.85	−0.00942	−0.00826	−0.00714	−0.00606	−0.00503	−0.00404	−0.00297			
0.90	−0.00953	−0.00838	−0.00727	−0.00622	−0.00522	−0.00426	−0.00334	−0.00238		
0.95	−0.00961	−0.00846	−0.00736	−0.00632	−0.00533	−0.00440	−0.00351	−0.00267	−0.00180	
1.00	−0.00965	−0.00851	−0.00741	−0.00638	−0.00540	−0.00448	−0.00361	−0.00279	−0.00200	−0.00123

Table 6 Calibration matrix $\overline{b}_{ij}$ for thickness $t = 1.50$ mm

Stress depth										
Hole depth										
mm	0.05	0.1	0.15	0.2	0.25	0.3	0.35	0.4	0.45	0.5
0.05	−0.01508									
0.10	−0.01759	−0.01625								
0.15	−0.01965	−0.01874	−0.01690							
0.20	−0.02172	−0.02092	−0.01967	−0.01728						
0.25	−0.02365	−0.02287	−0.02167	−0.01998	−0.01725					
0.30	−0.02531	−0.02457	−0.02350	−0.02199	−0.01996	−0.01696				
0.35	−0.02682	−0.02611	−0.02509	−0.02370	−0.02191	−0.01972	−0.01653			
0.40	−0.02819	−0.02749	−0.02650	−0.02516	−0.02350	−0.02153	−0.01920	−0.01593		
0.45	−0.02944	−0.02875	−0.02775	−0.02646	−0.02490	−0.02307	−0.02095	−0.01850	−0.01524	
0.50	−0.03047	−0.02982	−0.02887	−0.02760	−0.02607	−0.02434	−0.02240	−0.02022	−0.01773	−0.01446
0.55	−0.03143	−0.03080	−0.02986	−0.02862	−0.02713	−0.02545	−0.02359	−0.02156	−0.01932	−0.01683
0.60	−0.03227	−0.03166	−0.03074	−0.02951	−0.02805	−0.02641	−0.02461	−0.02266	−0.02057	−0.01832
0.65	−0.03303	−0.03242	−0.03151	−0.03031	−0.02885	−0.02724	−0.02548	−0.02359	−0.02158	−0.01948
0.70	−0.03367	−0.03308	−0.03218	−0.03099	−0.02955	−0.02796	−0.02623	−0.02437	−0.02242	−0.02040
0.75	−0.03424	−0.03366	−0.03277	−0.03158	−0.03016	−0.02859	−0.02688	−0.02505	−0.02314	−0.02118
0.80	−0.03472	−0.03416	−0.03328	−0.03210	−0.03069	−0.02913	−0.02744	−0.02563	−0.02375	−0.02183
0.85	−0.03515	−0.03460	−0.03373	−0.03256	−0.03116	−0.02961	−0.02793	−0.02614	−0.02429	−0.02239
0.90	−0.03552	−0.03498	−0.03412	−0.03296	−0.03156	−0.03002	−0.02836	−0.02658	−0.02474	−0.02287
0.95	−0.03584	−0.03531	−0.03446	−0.03330	−0.03192	−0.03038	−0.02873	−0.02696	−0.02514	−0.02328
1.00	−0.03612	−0.03559	−0.03475	−0.03360	−0.03222	−0.03069	−0.02905	−0.02729	−0.02548	−0.02364
Stress depth										
Hole depth										
mm	0.55	0.60	0.65	0.70	0.75	0.80	0.85	0.90	0.95	1.00
0.55	−0.01364									
0.60	−0.01587	−0.01280								
0.65	−0.01727	−0.01491	−0.01196							
0.70	−0.01833	−0.01618	−0.01391	−0.01112						
0.75	−0.01919	−0.01718	−0.01512	−0.01296	−0.01033					
0.80	−0.01989	−0.01796	−0.01602	−0.01406	−0.01202	−0.00954				
0.85	−0.02050	−0.01862	−0.01676	−0.01491	−0.01306	−0.01114	−0.00881			
0.90	−0.02100	−0.01915	−0.01734	−0.01557	−0.01382	−0.01208	−0.01028	−0.00811		
0.95	−0.02143	−0.01962	−0.01784	−0.01611	−0.01443	−0.01279	−0.01116	−0.00947	−0.00746	
1.00	−0.02180	−0.02001	−0.01826	−0.01657	−0.01493	−0.01335	−0.01180	−0.01027	−0.00871	−0.00684

Table 7 Calibration matrix $\bar{a}_{ij}$ for thickness $t = 2.00$ mm

Stress depth										
Hole depth										
mm	0.05	0.1	0.15	0.2	0.25	0.3	0.35	0.4	0.45	0.5
0.05	−0.00751									
0.10	−0.00909	−0.00800								
0.15	−0.01041	−0.00960	−0.00825							
0.20	−0.01162	−0.01080	−0.00985	−0.00829						
0.25	−0.01271	−0.01190	−0.01097	−0.00987	−0.00816					
0.30	−0.01369	−0.01286	−0.01197	−0.01092	−0.00971	−0.00789				
0.35	−0.01455	−0.01372	−0.01283	−0.01184	−0.01069	−0.00939	−0.00753			
0.40	−0.01532	−0.01447	−0.01358	−0.01261	−0.01153	−0.01031	−0.00896	−0.00709		
0.45	−0.01598	−0.01513	−0.01424	−0.01327	−0.01221	−0.01107	−0.00980	−0.00844	−0.00660	
0.50	−0.01656	−0.01569	−0.01480	−0.01383	−0.01280	−0.01168	−0.01050	−0.00921	−0.00786	−0.00608
0.55	−0.01705	−0.01618	−0.01528	−0.01432	−0.01329	−0.01219	−0.01104	−0.00984	−0.00857	−0.00725
0.60	−0.01746	−0.01659	−0.01568	−0.01472	−0.01370	−0.01261	−0.01148	−0.01032	−0.00912	−0.00789
0.65	−0.01781	−0.01693	−0.01602	−0.01506	−0.01404	−0.01296	−0.01185	−0.01071	−0.00955	−0.00838
0.70	−0.01809	−0.01721	−0.01630	−0.01534	−0.01432	−0.01325	−0.01215	−0.01102	−0.00988	−0.00875
0.75	−0.01833	−0.01745	−0.01654	−0.01557	−0.01456	−0.01349	−0.01239	−0.01127	−0.01015	−0.00905
0.80	−0.01852	−0.01764	−0.01673	−0.01576	−0.01475	−0.01368	−0.01259	−0.01148	−0.01037	−0.00927
0.85	−0.01868	−0.01779	−0.01688	−0.01592	−0.01490	−0.01384	−0.01275	−0.01164	−0.01054	−0.00946
0.90	−0.01880	−0.01792	−0.01700	−0.01604	−0.01502	−0.01396	−0.01287	−0.01177	−0.01067	−0.00960
0.95	−0.01890	−0.01801	−0.01710	−0.01613	−0.01512	−0.01406	−0.01297	−0.01187	−0.01078	−0.00971
1.00	−0.01897	−0.01809	−0.01717	−0.01621	−0.01519	−0.01414	−0.01305	−0.01195	−0.01086	−0.00980
Stress depth										
Hole depth										
mm	0.55	0.60	0.65	0.70	0.75	0.80	0.85	0.90	0.95	1.00
0.55	−0.00556									
0.60	−0.00662	−0.00503								
0.65	−0.00719	−0.00600	−0.00452							
0.70	−0.00763	−0.00651	−0.00539	−0.00403						
0.75	−0.00796	−0.00690	−0.00585	−0.00481	−0.00357					
0.80	−0.00821	−0.00718	−0.00618	−0.00521	−0.00426	−0.00314				
0.85	−0.00840	−0.00739	−0.00643	−0.00551	−0.00461	−0.00375	−0.00274			
0.90	−0.00856	−0.00756	−0.00661	−0.00571	−0.00487	−0.00405	−0.00327	−0.00237		
0.95	−0.00868	−0.00769	−0.00675	−0.00587	−0.00504	−0.00427	−0.00353	−0.00283	−0.00203	
1.00	−0.00877	−0.00778	−0.00686	−0.00599	−0.00517	−0.00442	−0.00371	−0.00305	−0.00242	−0.00172

Table 8 Calibration matrix $\overline{b}_{ij}$ for thickness $t = 2.00$ mm

Stress depth										
Hole depth										
mm	0.05	0.1	0.15	0.2	0.25	0.3	0.35	0.4	0.45	0.5
0.05	−0.01414									
0.10	−0.01653	−0.01532								
0.15	−0.01846	−0.01768	−0.01598							
0.20	−0.02043	−0.01976	−0.01864	−0.01638						
0.25	−0.02226	−0.02161	−0.02055	−0.01898	−0.01637					
0.30	−0.02384	−0.02323	−0.02230	−0.02091	−0.01899	−0.01611				
0.35	−0.02526	−0.02469	−0.02380	−0.02253	−0.02086	−0.01878	−0.01570			
0.40	−0.02654	−0.02598	−0.02512	−0.02391	−0.02237	−0.02053	−0.01831	−0.01514		
0.45	−0.02773	−0.02717	−0.02631	−0.02515	−0.02371	−0.02199	−0.01999	−0.01765	−0.01448	
0.50	−0.02870	−0.02818	−0.02736	−0.02623	−0.02482	−0.02320	−0.02138	−0.01930	−0.01691	−0.01374
0.55	−0.02960	−0.02910	−0.02829	−0.02718	−0.02581	−0.02425	−0.02250	−0.02058	−0.01844	−0.01605
0.60	−0.03040	−0.02991	−0.02912	−0.02803	−0.02668	−0.02516	−0.02347	−0.02162	−0.01963	−0.01748
0.65	−0.03109	−0.03062	−0.02984	−0.02876	−0.02743	−0.02593	−0.02429	−0.02250	−0.02059	−0.01859
0.70	−0.03168	−0.03123	−0.03046	−0.02939	−0.02808	−0.02660	−0.02499	−0.02324	−0.02138	−0.01946
0.75	−0.03221	−0.03176	−0.03101	−0.02995	−0.02864	−0.02719	−0.02559	−0.02387	−0.02206	−0.02019
0.80	−0.03266	−0.03222	−0.03148	−0.03043	−0.02913	−0.02769	−0.02611	−0.02441	−0.02263	−0.02080
0.85	−0.03305	−0.03262	−0.03188	−0.03084	−0.02956	−0.02812	−0.02655	−0.02487	−0.02311	−0.02131
0.90	−0.03339	−0.03297	−0.03224	−0.03120	−0.02992	−0.02850	−0.02694	−0.02527	−0.02353	−0.02175
0.95	−0.03369	−0.03328	−0.03255	−0.03152	−0.03025	−0.02883	−0.02728	−0.02561	−0.02388	−0.02212
1.00	−0.03394	−0.03353	−0.03281	−0.03178	−0.03052	−0.02910	−0.02756	−0.02591	−0.02419	−0.02244
Stress depth										
Hole depth										
mm	0.55	0.60	0.65	0.70	0.75	0.80	0.85	0.90	0.95	1.00
0.55	−0.01297									
0.60	−0.01513	−0.01216								
0.65	−0.01647	−0.01420	−0.01137							
0.70	−0.01749	−0.01544	−0.01327	−0.01058						
0.75	−0.01830	−0.01638	−0.01442	−0.01236	−0.00984					
0.80	−0.01896	−0.01712	−0.01527	−0.01341	−0.01147	−0.00911				
0.85	−0.01951	−0.01772	−0.01595	−0.01420	−0.01244	−0.01063	−0.00843			
0.90	−0.01997	−0.01821	−0.01649	−0.01481	−0.01316	−0.01151	−0.00982	−0.00778		
0.95	−0.02036	−0.01864	−0.01695	−0.01531	−0.01372	−0.01217	−0.01064	−0.00907	−0.00718	
1.00	−0.02070	−0.01899	−0.01732	−0.01572	−0.01417	−0.01268	−0.01123	−0.00981	−0.00835	−0.00662

References

1. Webster GA, Ezeilo AN (2001) Residual stress distributions and their influence on fatigue lifetimes. Int J Fatigue 23:375–383. https://doi.org/10.1016/S0142-1123(01)00133-5
2. Barsoum Z (2008) Residual stress analysis and fatigue of multi-pass welded tubular structures. Eng Fail Anal 15(7):863–874. https://doi.org/10.1016/j.engfailanal.2007.11.016
3. Moen CD, Igusa T, Schafer BW (2008) Prediction of residual stresses and strains in cold-formed steel members. Thin-Walled Struct 46(11): 1274–1289. https://doi.org/10.1016/j.tws.2008.02.002
4. Heinilä S, Marquis GB, Björk T (2008) Observations on fatigue crack paths in the corners of cold-formed high-strength steel tubes. Eng Fract Mech 75(3):833–844. https://doi.org/10.1016/j.engfracmech.2007.01.010
5. Díaz A, Cuesta II, Alegre JM (2017) A methodology for the numerical assessment of autofrettage influence on hydrogen content near a notch in a 4130 steel pressure vessel. Theor Appl Fract Mech 92:205–213. https://doi.org/10.1016/j.tafmec.2017.07.024
6. Blasón S, Rodríguez C, Belzunce J, Suárez C (2017) Fatigue behaviour improvement on notched specimens of two different steels through deep rolling, a surface cold treatment. Theor Appl Fract Mech 92:223–228. https://doi.org/10.1016/j.tafmec.2017.08.003
7. Alegre JM, Bravo P, Preciado M (2007) Fatigue behaviour of an autofrettaged high-pressure vessel for the food industry. Eng Fail Anal 14(2):396–407. https://doi.org/10.1016/j.engfailanal.2006.02.015

8. Rossini NS, Dassisti M, Benyounis KY, Olabi AG (2012) Methods of measuring residual stresses in components. Mater Des 35:572–588. https://doi.org/10.1016/j.matdes.2011.08.022
9. Schajer GS (2010) Advances in hole-drilling residual stress measurements. Exp Mech 50(2):159–168. https://doi.org/10.1007/s11340-009-9228-7
10. ASTM E837 - 13a (2013) Standard test method for determining residual stresses by the hole-drilling strain-gage method. ASTM International, West Conshohocken
11. Beghini M, Bertini L, Santus C (2010) A procedure for evaluating high residual stresses using the blind hole drilling method, including the effect of plasticity. J Strain Anal Eng Des 45(4):301–318. https://doi.org/10.1243/03093247jsa579
12. Nobre JP, Kornmeier M, Scholtes B (2018) Plasticity effects in the hole-drilling residual stress measurement in peened surfaces. Exp Mech 58(2):369–380. https://doi.org/10.1007/s11340-017-0352-5
13. Beghini M, Bertini L (1998) Recent advances in the hole drilling method for residual stress measurement. J Mater Eng Perform 7(2):163. https://doi.org/10.1361/105994998770347882
14. Beghini M, Bertini L, Mori LF (2010) Evaluating non-uniform residual stress by the hole-drilling method with concentric and eccentric holes. Part II: application of the influence functions to the inverse problem. Strain 46(4):337–346. https://doi.org/10.1111/j.1475-1305.2009.00684.x
15. Schajer GS (1988) Measurement of non-uniform residual stresses using the hole-drilling method. Part I—stress calculation procedures. J Eng Mater Technol 110(4):338–343. https://doi.org/10.1115/1.3226059
16. Niku-Lari A, Lu J, Flavenot JF (1985) Measurement of residual-stress distribution by the incremental hole-drilling method. J Mech Work Technol 11(2):167–188. https://doi.org/10.1016/0378-3804(85)90023-3
17. Schajer GS, Prime MB (2006) Use of inverse solutions for residual stress measurements. J Eng Mater Technol 128(3):375–382. https://doi.org/10.1115/1.2204952
18. Zuccarello B (1999) Optimal calculation steps for the evaluation of residual stress by the incremental hole-drilling method. Exp Mech 39(2):117–124. https://doi.org/10.1007/bf02331114
19. Schajer GS (2010) Hole-drilling residual stress measurements at 75: origins, advances, opportunities. Exp Mech 50(2):245–253. https://doi.org/10.1007/s11340-009-9285-y
20. Schuster S, Steinzig M, Gibmeier J (2017) Incremental hole drilling for residual stress analysis of thin walled components with regard to plasticity effects. Exp Mech 57(9):1457–1467. https://doi.org/10.1007/s11340-017-0318-7
21. Schajer GS (1988) Measurement of non-uniform residual stresses using the hole-drilling method. Part II—practical application of the integral method. J Eng Mater Technol 110(4):344–349. https://doi.org/10.1115/1.3226060
22. Beghini M, Bertini L (2000) Analytical expressions of the influence functions for accuracy and versatility improvement in the hole-drilling method. J Strain Anal Eng Des 35(2):125–135. https://doi.org/10.1243/0309324001514071
23. Aoh J-N, Wei C-S (2002) On the improvement of calibration coefficients for hole-drilling integral method: part I—analysis of calibration coefficients obtained by a 3-D FEM model. J Eng Mater Technol 124(2):250–258. https://doi.org/10.1115/1.1416685
24. Xiao B, Li K, Rong Y (2011) Automatic determination and evaluation of residual stress calibration coefficients for hole-drilling strain gauge integral method. Strain 47(s1):e525–e534. https://doi.org/10.1111/j.1475-1305.2009.00650.x
25. Zhu X, di Scalea FL (2017) Thermal stress measurement in continuous welded rails using the hole-drilling method. Exp Mech 57(1):165–178
26. Schajer GS, Abraham C (2014) Residual stress measurements in finite-thickness materials by hole-drilling. Exp Mech 54(9):1515–1522. https://doi.org/10.1007/s11340-014-9935-6